Journal of Materials Chemistry C

ROYAL SOCIETY OF CHEMISTRY

PAPER

View Article Online
View Journal | View Issue

Cite this: J. Mater. Chem. C, 2025, 13, 5279

Assembly of van der Waals structure from CVD-grown 2-dimensional materials using plasma-treated polyvinyl chloride†

Bin Xu,‡[ab] Satoru Masubuchi,‡[c] Yusai Wakafuji,[c] Yuanzhe Li,[a] Tomoki Machida*[c] and Junichiro Shiomi *[ab]

Two-dimensional (2D) van der Waals (vdW) stacking structures have gathered significant attention owing to their unique properties. The practical and large-scale applications of 2D materials in advanced technologies significantly hinge on the efficient transfer of chemical vapor deposition (CVD) synthesized 2D materials. However, this is hindered by issues such as contamination, limited materials compliance, and restricted scalability. To address these issues, we developed an effective transfer method using plasma-treated polyvinyl chloride (P-PVC) films and established a process for assembling vdW stack structures using a sequential pick-up procedure. Owing to the enhanced surface adhesion achieved using the plasma, P-PVC can overcome the strong adhesion between CVD-synthesized 2D materials and substrates. Consequently, P-PVC exhibited exceptional performance during the pick-up process with additional help of water delamination. The proposed method also showcases its advantages in the drop-off process, because the surface of P-PVC can act as a sacrificial layer that detaches from the PVC film along with the vdW structure. The P-PVC-based sequential pick-up approach not only mitigates interfacial contamination by polymer but can also play a vital role in facilitating efficient production and ensuring material compatibility. This technique offers significant potential for the physics and applications of vdW stacking structures.

Received 28th May 2024,
Accepted 10th January 2025

DOI: 10.1039/d4tc02204a

rsc.li/materials-c

Introduction

Two-dimensional (2D) atomically thin materials[1,2] have garnered significant attention owing to their unique structure and resultant novel properties.[3] They exhibit an absence of chemical bonding in the out-of-plane direction, enabling their assembly into stacked structures through van der Waals (vdW) interactions (vdW stacking), thereby circumventing the limitations of lattice matching.[3] They enable remarkable flexibility in material design, which has catalyzed a surge of research and yielded numerous discoveries on novel properties, such as superconducting,[4–6] highly efficient light-emitting,[7–10] detection,[11–13] and high-electron mobility.[14]

Considerable effort has been devoted to the fabrication of vdW stacks. Owing to the relatively limited and consistent interaction between the substrate and mechanically exfoliated 2D materials, extensive investigations have been conducted on the transfer of exfoliated 2D materials for vdW stacking and reliable techniques for such transfers have been established. It has been demonstrated that various types of polymers are effective for transferring mechanically exfoliated 2D materials, including polymethyl methacrylate (PMMA),[15–17] Elvacite,[18,19] polyvinyl chloride (PVC),[20–22] polycarbonate (PC),[23] polypropylene carbonate,[24,25] and polydimethylsiloxane (PDMS).[26,27]

The advancement of chemical vapor deposition (CVD) technology has revolutionized the large-scale synthesis of 2D materials.[28–30] Large-scale production of vdW structures can be achieved using CVD-synthesized 2D materials, thereby potentially promoting additional prospects for the practical applications of 2D materials. However, compared to exfoliated 2D materials, CVD-grown 2D materials exhibit a significantly stronger interaction with the substrates. This interaction significantly depends on the synthesis temperature. Furthermore, the reported variations in the interaction with the synthesis temperature differ among studies. In addition, the presence of residual ingredients in CVD-synthesized 2D materials weaken the adhesion of the materials to the polymer used for transfer. Consequently, CVD-grown 2D materials are significantly more difficult to transfer than their mechanically exfoliated counterparts.[31] One common solution to this issue is to weaken the interaction between the 2D materials and substrate.

[a] Department of Mechanical Engineering, The University of Tokyo, 7-3-1 Hongo, Bunkyo, Tokyo, 113-8656, Japan. E-mail: shiomi@photon.t.u-tokyo.ac.jp
[b] Institute of Engineering Innovation, The University of Tokyo, 2-11 Yayoi, Bunkyo, Tokyo, 113-8656, Japan
[c] Institute of Industrial Science, The University of Tokyo, 4-6-1 Komaba, Meguro-ku, Tokyo, 153-8505, Japan. E-mail: tmachida@iis.u-tokyo.ac.jp

† Electronic supplementary information (ESI) available. See DOI: https://doi.org/10.1039/d4tc02204a

‡ These authors contributed equally: Bin Xu, Satoru Masubuchi.

With SiO_2/Si substrates, this is achieved by etching the SiO_2 layer of the substrate using NaOH[32] and KOH.[33] Additionally, water-soluble substrates, such as NaCl or NaS_x,[34] can be dissolved. However, these methods are only applicable with particular substrates. Additionally, the pick-up method employed may damage the substrates, rendering them non-reusable. In addition, these methods typically adopt a wet pick-up process, which involves complex and time-consuming procedures, including spin coating, baking, and etching. These disadvantages limit their applications in the fabrication and mass production of multilayered vdW structures.

An alternative method is to improve the adhesion between 2D materials and the polymer surface, which can be achieved by coating an additional thin layer of polymer, such as dimethyl sulfoxide,[35] polyvinyl alcohol (PVA),[36] ethylene vinyl acetate (EVA),[37] and polyvinylpyrrolidone,[38] on PDMS, polyethylene terephthalate (PET), and PVA films. These hybrid polymer films can be used to transfer 2D materials *via* a dry pick-up process, which is easier to use during mass production. Hong *et al.* demonstrated a roll-to-roll transfer using a PET/EVA film.[39] Nevertheless, as the adhesion depends on CVD growth conditions, it may result in an excessive adhesion between the 2D materials and substrates. In such cases, additional procedures, such as water intercalation[37,40] and heating,[35] are required to weaken the adhesion.

However, an enhanced adhesion between the polymer and 2D materials inevitably leads to the presence of residual polymer on the surface of the 2D materials after drop-off. These residuals may contaminate the interface between the 2D materials when the vdW stacks are fabricated *via* conventional individual transfer. A radical way to address these issues is to fabricate multilayer vdW structures using a sequential pick-up method. However, to date, only few studies have achieved the sequential pick-up of CVD-grown 2D materials. Table S1 (ESI†) presents a comparison between previous transfer methods discussed above. Notably, transfer of 2D materials like graphene that grown on metal substrate is quite different from those on grown on dielectric substrates, and we do not include them in the comparison because they are almost impossible to be picked up *via* a dry process that we are aiming for.

In this study, we develop a highly efficient and versatile sequential pick-up method for assembling CVD-synthesized 2D materials into vdW structures using a plasma-treated PVC film (P-PVC). Plasma treatment can be used to generate a sacrificial layer composed of PVC with a low molecular weight and hydrophilic surface. This method can enhance the adhesion between CVD-grown 2D materials and the sacrificial layer, enabling the fabrication of stacking structure using a sequential pick-up method. The sacrificial layer is also beneficial for dropping off the vdW structure to the target substrate. It is a highly versatile method well-suited for a diverse range of 2D materials, substrates, and surface conditions, demonstrating its significant potential for various vdW-structure applications.

Experimental methods

Transferring CVD-synthesized 2D materials using P-PVC

Fig. 1(a) and (b) show a schematic of the transfer method for assembling vdW heterostructures. The stamp used for the 2D-material transfer comprised a thin PVC film, PDMS dome, and gel sheet. The PDMS dome is used to achieve precise spatial manipulation of 2D materials with minimal contact area and improved pick-up efficiency due to its softness compared to PVC film. The selection of the type of PDMS dome depends on the size of the target 2D material and can be customized to be either micro or normal shaped.[21] The stamp was treated with plasma to modify the surface layer of the PVC film. Herein, we used a ICP plasma (Harrick Plasma, PDC-32G) generated using a radio-frequency power supply of 10.5 W after back pumping the chamber from atmospheric pressure to a vacuum of approximately 280 Pa without introducing other gas. The plasma was lasted for 40 s (details regarding the preparation of the P-PVC stamp and the optimization of the plasma parameters are provided in the ESI:† Methods section). The plasma treatment enhanced the ability of the stamp to pick up CVD-synthesized 2D materials and assisted in the release of vdW structures from the PVC film during their drop-off. As will be discussed later, the top P-PVC layer is critical as it releases the 2D materials from the stamp during the drop-off, acting like a ''sacrificial layer''. The structural characterization of the P-PVC sacrificial layer and its contribution to the transfer process will be discussed in the following section. In contrast, we encountered problems when dropping off CVD synthesized 2D materials using pristine PVC.

Using this P-PVC stamp, we could effectively transfer CVD-synthesized 2D materials of different types of substrates. For example, we performed the transfer of both WS_2-on-sapphire and MoS_2-on-SiO_2 sample to either sapphire or SiO_2 substrate with almost 100% successful rate under the optimized parameters (the details of CVD synthesis of WS_2 and MoS_2 is illustrated in ESI:† Methods; in this work, the substrate of MoS_2 and WS_2 are fixed to be SiO_2 and sapphire, respectively). Notably, this method is useful especially for those 2D materials can be grown directly on the dielectric substrates like sapphire and SiO_2, while it is not suitable for materials like graphene that synthesized on metal substrates.

Fig. 1(c)–(e) shows a schematic of the transfer process. Using P-PVC, we picked up 2D materials at temperature range of 60–110 °C, where the P-PVC becomes softer and facilitate a better contact between 2D materials and P-PVC for the pick-up manipulation. Fig. 1(d) shows a representative optical image of a monolayer MoS_2 picked up on a P-PVC stamp from a SiO_2 substrate. For the CVD synthesized MoS_2 on SiO_2, and WS_2 on sapphire used in present study, approximately 100% pick-up rate was achieved when using P-PVC and water delamination, while pristine PVC sometimes can only partially pick up the 2D materials. It should be noted that a 100% pick-up indicates that all the 2D materials on the substrate can be picked up during the stamping process. This high efficiency is due to the increased adhesion of P-PVC and the reduced adhesion between the 2D materials and the substrates, caused by water delamination. The comparison of the PVC and P-PVC in details will be discussed later. For the multi-layer stacking, we repeated the pick-up manipulation to sequentially pick the 2D materials and assemble the vdW stacking on the stamp. The picked-up

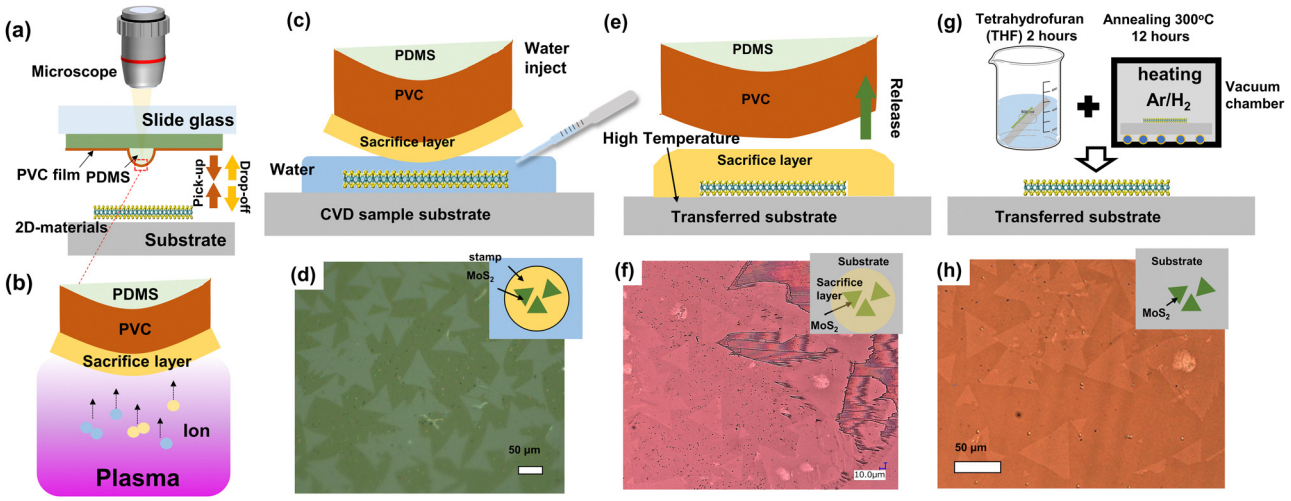

Fig. 1 Transfer of 2D materials by P-PVC. Schematics of (a) the transfer setup and (b) plasma-treated P-PVC. (c) Schematic of pick-up of 2D materials assisted by water delamination, and (d) a representative optical image of a CVD-grown monolayer MoS_2 picked up on the P-PVC stamp. (e) Schematic of drop-off of 2D materials onto the target substrate using a sacrificial layer, and (f) a representative optical image of a monolayer MoS_2 dropped off onto a sapphire substrate showing residual PVC on the surface. (g) Schematic of the cleaning procedure for the removal of sacrificial layer, and (h) a representative optical image of a transferred monolayer MoS_2 on a sapphire substrate after the cleaning process.

2D materials were then dropped off onto the targeted substrate at temperatures ranging from 150 to 170 °C (Fig. 1(e)). At such temperatures, which are higher than the melting point of the sacrificial layer, the PVC with the attached 2D materials melts and detaches from the PVC film. The sacrificial layer on the 2D materials was then removed *via* a cleaning procedure (Fig. 1(g)), which involved immersing the samples in a tetrahydrofuran (THF) solution and subsequently annealing them in an H_2/Ar atmosphere. Fig. 1(f) and (h) exhibit the monolayer MoS_2 after release and that after the following cleaning process, respectively. (More details of the transfer process will be discussed in ESI:† Method).

Results and discussion

Quality and versatility of 2D materials transferred by P-PVC

We also investigated the quality of the 2D materials after transfer manipulation. We compared the photoluminescence (PL) spectra of as-grown WS_2 on a sapphire substrate (Fig. 2(a)) with that transferred onto SiO_2/Si substrates using P-PVC (Fig. 2(b)) and the commonly used PMMA (Fig. 2(c)). As shown in the PL spectrum (Fig. 2(g)) and the corresponding PL intensity mapping (Fig. 2(b), (d), and (f)), the PL intensity remains almost unchanged after transfer using P-PVC and is higher than that transferred using PMMA. We also studied the PL intensity of MoS_2-on-SiO_2 and that transferred to a new SiO_2 substrate using P-PVC (Fig. S1, ESI†). The results revealed that the PL intensity of the P-PVC-transferred MoS_2 is comparable to that of the as-grown MoS_2.

The superiority of P-PVC also manifests in its compatibility with various 2D materials and substrates. Except for transferring MoS_2 from SiO_2 to sapphire substrate (Fig. 1) and WS_2 (from sapphire) and MoS_2 (from SiO_2) to SiO_2 substrate that demonstrated above, Fig. S2 (ESI†)/Fig. 3(a) shows the transferring of CVD-grown WS_2 from sapphire substrate and the assembly of bilayer vdW structure that released on sapphire and SiO_2 substrate, respectively. Fig. S3 (ESI†) shows the assembly of a vdW heterostructure using a mixture of CVD-grown and mechanically exfoliated 2D materials.

Interlayer interaction in vdW structures assembly by P-PVC

The sequential pick-up process ensures the avoidance of a direct contact between the polymer and 2D materials interface, thereby guaranteeing a relatively clean interfaces that free of polymer residual between individual 2D layers, which are imperative for

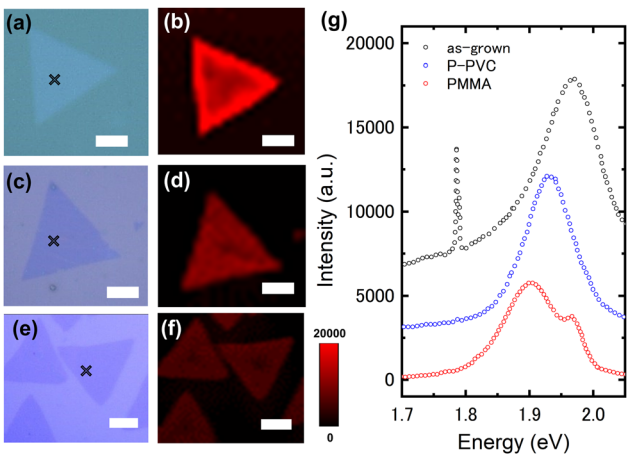

Fig. 2 Characterization of the quality of 2D materials after the transfer process. Optical image of a CVD synthesized monolayer WS_2 (a) on a sapphire substrate and after being transferred using (c) P-PVC and (e) PMMA onto an SiO_2 substrate. Corresponding PL mapping of the monolayer WS_2 (b) before and after transfer using (d) P-PVC and (f) PMMA, and (g) the representative PL spectrum at the marked points in (a), (c), and (e). (Scale bar is 10 μm.)

investigating the physics of interlayer interaction effects. Notably, the interfacial cleanliness also strongly depends on other experimental conditions like the transfer environment and the sample quality of the 2D materials. For example, the adsorption of water and amorphous carbon, and the residual of the CVD precursor on the 2D materials, and the wrinkle of the 2D materials can degraded the interfacial quality. Nevertheless, limited by the other transfer conditions like the circumstances (exp. transfer in vacuum chamber are with less bubbles[41]), and the quality of the CVD samples, we found some bubbles and wrinkles in the bilayer region from the AFM measurement (Fig. S4, ESI†), which required extra effort to deal with. However, we can see from the AFM results that the monolayer region is quite clean, reflecting little polymer residual on the top of the 2D materials after transfer.

To elucidate the interlayer interaction of the vdW structures, we investigated the PL and Raman spectra of bilayer WS_2. Measurement details are provided in ESI:† Methods section. Fig. 3(a) exhibit a low-magnification optical image of bilayer WS_2 by sequentially picking up CVD-grown WS_2 from sapphire substrates for twice after dropped onto SiO_2/Si substrates. Fig. 3(b) shows the representative PL spectra of a monolayer WS_2 and bilayer WS_2 with twist angles of 2° and 31°. The PL spectrum of bilayer WS_2 with other twist angles is shown in Fig. S5 (ESI†). Compared to monolayer WS_2, the bilayer WS_2 exhibits broader PL peaks. In particular, when the twist angle is close to 0° and 60°, the indirect band transfer peak due to the interlayer exciton transfer appears at a relatively low energy of approximately 1.6 eV,[42] accompany with the pronounced suppression of the PL peaks to 1/20 of those of monolayer WS_2. Fig. 3(c) shows the integrated peak intensities of bilayer WS_2 with different twist angles. Evidently, the intensity varies with variations in the twist angle, which is well-consistent with the results of a previous study conducted on twisted bilayer MoS_2 directly synthesized using the CVD method.[42] We also performed PL mapping analysis on bilayer WS_2 with twist angles of 57°. The bilayer region exhibits significantly suppressed PL. By contrast, monolayer region exhibits a vigorous PL intensity (Fig. 3(d)). Fig. S6 (ESI†) shows the PL mapping of WS_2 with a twist angle of 2°, where same conclusion can be drawn. Fig. 3(f) shows the Raman spectra of bilayer WS_2 with different twist angles. The Raman spectra of bilayer WS_2 with other twist angles are shown in Fig. S7 (ESI†). The peaks at approximately 352 cm^{-1} and 418 cm^{-1} represent the E_{1g} and A_{1g} optical phonons, respectively, and are highly sensitive to the twist angle. For twist angles near 0° and 60°, a significant upshift and downshift of the E_{1g} and A_{2g} peaks are observed, respectively. The influence of the twist angle on E_{1g} and A_{1g} peaks indicates an evident variation in interlayer interactions, which is well-consistent with previous studies on twisted bilayer WS_2 fabricated using the PMMA stamping method.[43] Overall, the clear twist-angle dependence in the PL and Raman spectra indicates favorable interlayer interactions with respect to the electron and phonon properties, suggesting the advantages of the proposed sequential pick-up method using P-PVC.

The characterization of the P-PVC and its critical role in transferring CVD synthesized 2D materials

To understand the critical role of the plasma treatment of PVC in assisting the transfer process, we systematically investigated the structural variations in PVC due to plasma treatment and their influence on the transfer process, with a particular focus on the top P-PVC layer, also known as the sacrificial layer in the drop-off process. Initially, we measured the contact angle of

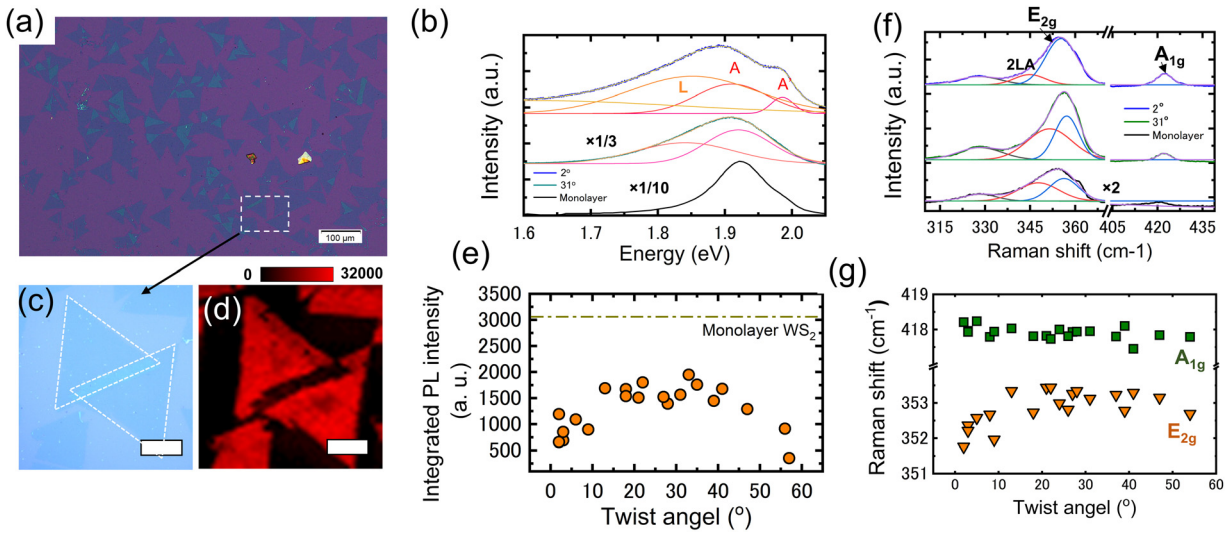

Fig. 3 Assembly 2D vdW stacking using plasma-treated PVC (P-PVC) stamp. (a) Optical image of transferred twist bilayer WS_2. (b) PL spectrum of monolayer and bilayer WS_2 with twist angle of 2° and 31°. The spectrum intensities of the monolayer WS_2 and bilayer WS_2 were multiplied by 1/10 and 1/3, respectively; red, pink, and brown curve is the Gaussian fitting of the experimental data. (c) Representative optical image of a bilayer WS_2 with a twist angle of 57° and (d) the corresponding PL intensity mapping (the region marked in (a), scale bar is 20 μm in (c) and (d)). (e) Integrated PL intensity of WS_2 with different twist angles. (f) Raman spectrum of monolayer WS_2 and bilayer WS_2 with twist angles of 2° and 31°; green, red, blue, and purple curves are the Gaussian fitting of the experimental data, intensity of the spectrum of monolayer WS_2 was multiplied by 2. (g) Peak position of A_{1g} and E_{2g} modes of bilayer WS_2 with different twist angles.

deionized (DI) water on PVC and P-PVC films to evaluate the change in the surface energy of PVC, a crucial factor associated with surface adhesion and closely correlated with pick-up manipulation (Fig. 4(a)). The contact angle decreases from 80° for the pristine PVC film to approximately 54° for the P-PVC film, indicating an enhanced adhesion for the P-PVC film. This enhancement in hydrophilicity well-aligns with previous studies. It is typically attributed to the generation of hydroxyl (–OH), carbonyl (–C═O), and vinyl (–CH═CH_2) bonds on the surface.[44] As CVD-grown 2D materials exhibit significantly stronger interaction with the substrates ($E_{2d\text{-}sub}$), the improved surface adhesion of P-PVC can promote the interaction between the 2D materials and stamp ($E_{2d\text{-}pvc}$). For example, this enables the pick-up of CVD-synthesized WS_2/MoS_2 at temperatures as low as 50 °C, which cannot be achieved using pristine PVC unless the temperature exceeds 70 °C. The enhanced $E_{2d\text{-}pvc}$ significantly facilitates the pick-up process, demonstrating the remarkable adaptability to various CVD-synthesized 2D materials on different substrates. This is particularly advantageous given the strong and variable adhesion characteristics typically observed between CVD-synthesized 2D materials and their substrates.

Moreover, when the P-PVC film was annealed under 170 °C, which is the drop-off temperature, the contact angle reverted to 72°. This suggests a decrease in the surface adhesion. As indicated in previous studies, the contact angle slowly increases after plasma treatment owing to the unstable surface conditions created by the plasma.[45] High temperatures significantly accelerate this increase. The weakened surface adhesion following high-temperature exposure can weaken the interactions between the P-PVC and the surface of 2D materials, reducing the amount of polymer residues after the drop-off and cleaning processes. Notably, the contact angle reflects only the properties of the top surface layer, extending to a depth of a few nanometers, which is preferentially modified by the plasma.

Using Fourier transform infrared (FTIR) measurements, we investigated the variations in the primary chemical components due to the plasma treatment. Using the ATR mode, where the penetration depth is approximately 810 nm for PVC, the characteristic vibration of the sacrificial layer on top of the PVC (Fig. 4(b)) can be identified. The representative modes at 2800–2900 cm^{-1} and 1425 cm^{-1} represent the stretching and symmetric in-plane bending vibrations of C–H, whereas those at 600–700 cm^{-1} represent the stretching mode of C–Cl. Despite changes in the overall intensity, the intensity of the individual modes varies to the same extent, indicating that the basic chemical component of the sacrificial layer, –[CH_2–CHCl]–, remains unchanged from that of pristine PVC. Notably, FTIR does not reflect surface chemical variations because the ATR unit used in the measurement has a large penetration depth of up to 2 μm, which is much thicker than the plasma-modified layer. This suggests that most of the P-PVC remains intact, with only the surface layer being modified through the formation of new chemical bonds. Besides, The FTIR intensity is primarily contingent on the concentration of the sample. As plasma may cause the surface roughening of PVC,[46] it may generate air gaps between the PVC film and diamond prism, thereby reducing the overall intensity of the individual peaks.

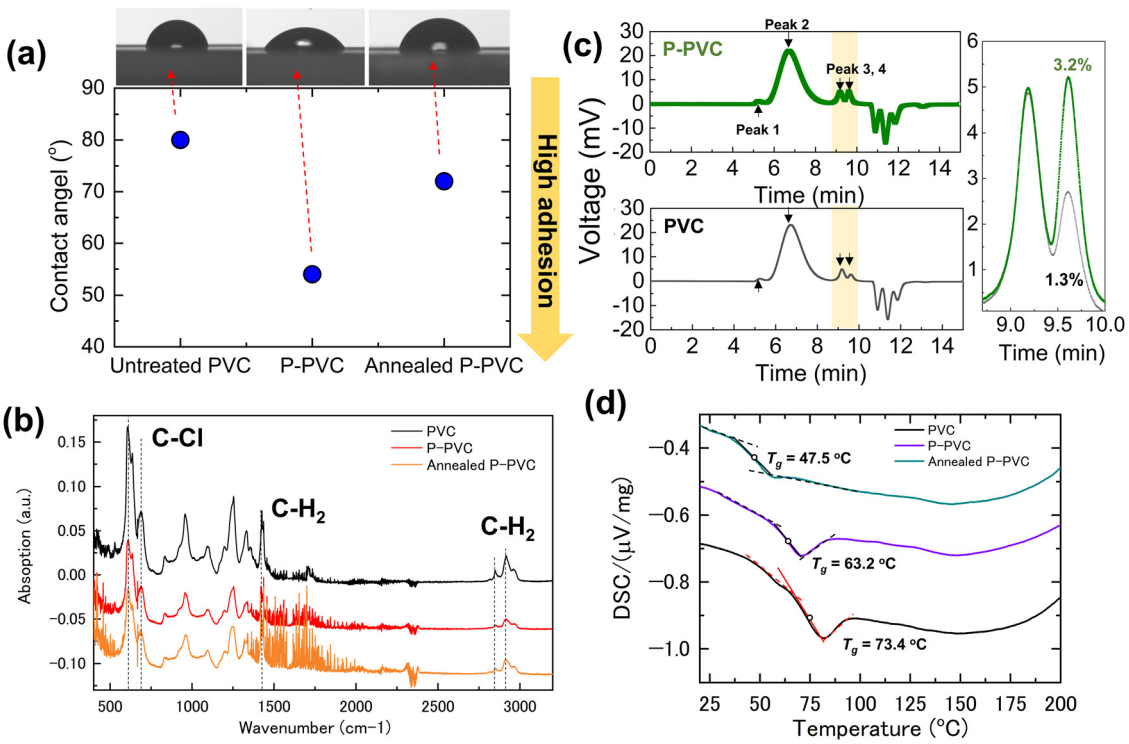

Fig. 4 Structure characterization of plasma-treated PVC (P-PVC) stamp. (a) DI water contact angle measurement, (b) FT-IR measurement, (c) gel filtration chromatography measurement, and (d) DSC measurement results of the pristine PVC, P-PVC, and annealed P-PVC film.

We identified the molecular weight of the PVC film, which can be used to determine the melting point. This may explain why the sacrificial layer melted at lower temperatures than the pristine PVC. We employed chromatography (see ESI:† Methods for details) to examine the molecular weight of PVC before and after the plasma treatment. Fig. 4(c) shows four characteristic peaks at different time points, which represent components with increased molecular weights from left to right: 1 813 859, 110 508, 1469, and 550 mol. The peak positions were similar for PVC before and after the plasma treatment. The difference occurs in the normalized proportion of peaks 2, 3, and 4: the normalized proportion of low-molecular-weight components (peaks 3 and 4) is approximately 2% higher in P-PVC (inset in Fig. 4(c)). As the plasma modified only the surface layer of the PVC film, the P-PVC sample included both plasma-treated and pristine-PVC. This implies that the change in the low-molecular-weight component of the plasma-treated PVC may be much more significant. The decrease in molecular weight may be caused by the scission of the polymer chains in PVC because high-energy radial and highly reactive plasma species can break the polymer chains of PVC.[47]

The variation in the structure of the PVC chain, as reflected by its molecular weight, also influences the glass transition temperature (T_g). The DSC results revealed that the T_g of PVC, P-PVC and annealed P-PVC films are 73.4 °C, 63.2 °C, and 47.5 °C, respectively. As the polymer softens when the temperature reaches its glass transition temperature,[19] the adhesion between the polymer and 2D materials is enhanced. Therefore, a reduction in T_g is advantageous to facilitate the pick-up of 2D materials at lower temperatures.

A decrease in molecular weight and the resultant low T_g are imperative to facilitate an efficient drop-off. Exfoliated 2D materials can be directly released onto the targeted substrates at the temperatures of 130–140 °C *via* a dry process. By contrast, we encountered difficulties in dropping off the CVD-grown 2D materials from the PVC film, even when the temperature was increased up to 200 °C, at which PVC films start to decompose. This difficulty is ascribed to the absorption of water during the delamination of the 2D materials and the introduction of impurities during CVD synthesis. These impurities adhere to the surface of the 2D materials, impeding their direct interaction with the intended substrate, thereby causing $E_{2d\text{-}pvc}$ to exceed $E_{2d\text{-}sub}$. This issue can be addressed by releasing the 2D materials with the sacrificial layer as the melting point was reduced to 150 °C, lower than the decomposition temperature. In this context, the magnitudes of $E_{2d\text{-}pvc}$ and $E_{2d\text{-}sub}$ are irrelevant. Fig. S8 (ESI†) shows temperature conditions and variations in $E_{2d\text{-}pvc}$ and $E_{2d\text{-}sub}$ during the transfer of the CVD-synthesized 2D and mechanically exfoliated materials using PVC and P-PVC stamps.

Conclusions

This paper presents an efficient and adaptable method for assembling van der Waals (vdW) heterostructures from CVD-grown 2D materials. The plasma-modified PVC (P-PVC) film enabled an efficient sequential pick-up, which guarantees clean interfaces and enables fast processing. Plasma treatment modified the surface of the PVC film, creating a sacrificial layer with improved surface adhesion. Aided by water-assisted delamination, the plasma treatment facilitated the sequential pick-up of various CVD-grown 2D materials from diverse substrates. The presence of the sacrificial layer enhanced the versatility of the drop-off process, enabling the release of 2D materials, regardless of their types, substrates, or surface conditions. Additionally, the adhesion of the P-PVC surface decreased upon heating, which enabled a facile removal of polymer residues from the 2D materials dropped onto the target substrate. We also verified the quality of the transferred 2D materials and vdW heterostructures through systematic characterization. The methodology developed in this study has potential applications in the fabrication of large-scale 2D-material systems. Furthermore, it can facilitate the development of advanced 2D vdW structure more efficiently and cost-effectively, thereby enabling promising mass production. However, we have pointed out that this method is not applicable for materials like CVD-synthesized graphene and BN that are grown on metal substrates, due to the very strong adhesion between the 2D materials and metal substrates and the failure of water delamination. Regarding the CVD growth technique for materials like graphene and BN, which is becoming increasingly mature and has significant potential for application, methods for their efficient transfer are critical, which requires extra innovation.

Author contributions

Bin Xu: conceptualization, visualization, validation, methodology, investigation, writing – original draft, funding acquisition. Satoru Masubuchi: validation, methodology, investigation. Yusai Wakafuji: investigation. Yuanzhe Li: methodology. Tomoki Machida: project administration, conceptualization, methodology, funding acquisition, writing – review & editing. Junichiro Shiomi: project administration, funding acquisition, writing – review & editing, conceptualization, visualization.

Data availability

The authors confirm that the data supporting the findings of this study are available within the article and its ESI.† Additional information related to present work are available on request from the corresponding author, Junichiro Shiomi and Tomoki Machida, upon reasonable request.

Conflicts of interest

The authors declare no conflict of interest.

Acknowledgements

This work was supported by JST-CREST (Grant number JPMJCR21O2, JPMJCR19I2), JST-Mirai (Grant number JPMJMI21G9),

and JSPS KAKENHI (Grant number 22K14189, 24K00817), and B. X. acknowledges support from the Hirose Foundation and Marubun Foundation.

References

1 K. S. Novoselov, A. K. Geim, S. V. Morozov, D. Jiang, Y. Zhang, S. V. Dubonos, I. V. Grigorieva and A. A. Firsov, *Science*, 2004, **306**, 666–669.
2 T. Cao, G. Wang, W. Han, H. Ye, C. Zhu, J. Shi, Q. Niu, P. Tan, E. Wang, B. Liu and J. Feng, *Nat. Commun.*, 2012, **3**, 887.
3 X. Li, L. Tao, Z. Chen, H. Fang, X. Li, X. Wang, J.-B. Xu and H. Zhu, *Appl. Phys. Rev.*, 2017, **4**, 021306.
4 N. Yabuki, R. Moriya, M. Arai, Y. Sata, S. Morikawa, S. Masubuchi and T. Machida, *Nat. Commun.*, 2016, **7**, 10616.
5 D. K. Efetov, L. Wang, C. Handschin, K. B. Efetov, J. Shuang, R. Cava, T. Taniguchi, K. Watanabe, J. Hone, C. R. Dean and P. Kim, *Nat. Phys.*, 2016, **12**, 328–332.
6 M. Kim, G. H. Park, J. Lee, J. H. Lee, J. Park, H. Lee, G. H. Lee and H. J. Lee, *Nano Lett.*, 2017, **17**, 6125–6130.
7 K. Tran, G. Moody, F. Wu, X. Lu, J. Choi, K. Kim, A. Rai, D. A. Sanchez, J. Quan, A. Singh, J. Embley, A. Zepeda, M. Campbell, T. Autry, T. Taniguchi, K. Watanabe, N. Lu, S. K. Banerjee, K. L. Silverman, S. Kim, E. Tutuc, L. Yang, A. H. MacDonald and X. Li, *Nature*, 2019, **567**, 71–75.
8 C. Jin, E. C. Regan, A. Yan, M. Iqbal Bakti Utama, D. Wang, S. Zhao, Y. Qin, S. Yang, Z. Zheng, S. Shi, K. Watanabe, T. Taniguchi, S. Tongay, A. Zettl and F. Wang, *Nature*, 2019, **567**, 76–80.
9 K. L. Seyler, P. Rivera, H. Yu, N. P. Wilson, E. L. Ray, D. G. Mandrus, J. Yan, W. Yao and X. Xu, *Nature*, 2019, **567**, 66–70.
10 E. M. Alexeev, D. A. Ruiz-Tijerina, M. Danovich, M. J. Hamer, D. J. Terry, P. K. Nayak, S. Ahn, S. Pak, J. Lee, J. I. Sohn, M. R. Molas, M. Koperski, K. Watanabe, T. Taniguchi, K. S. Novoselov, R. V. Gorbachev, H. S. Shin, V. I. Fal'ko and A. I. Tartakovskii, *Nature*, 2019, **567**, 81–86.
11 F. H. L. Koppens, T. Mueller, P. Avouris, A. C. Ferrari, M. S. Vitiello and M. Polini, *Nat. Nanotechnol.*, 2014, **9**, 780–793.
12 K. F. Mak and J. Shan, *Nat. Photonics*, 2016, **10**, 216–226.
13 Y. Wakafuji, R. Moriya, S. Park, K. Kinoshita, S. Masubuchi, K. Watanabe, T. Taniguchi and T. Machida, *Appl. Phys. Lett.*, 2019, **115**, 143101.
14 D. Rhodes, S. H. Chae, R. Ribeiro-Palau and J. Hone, *Nat. Mater.*, 2019, **18**, 541–549.
15 C. R. Dean, A. F. Young, I. Meric, C. Lee, L. Wang, S. Sorgenfrei, K. Watanabe, T. Taniguchi, P. Kim, K. L. Shepard and J. Hone, *Nat. Nanotechnol.*, 2010, **5**, 722–726.
16 A. Reina, H. Son, L. Jiao, B. Fan, M. S. Dresselhaus, Z. F. Liu and J. Kong, *J. Phys. Chem. C*, 2008, **112**, 17741–17744.
17 T. Uwanno, Y. Hattori, T. Taniguchi, K. Watanabe and K. Nagashio, *2D Mater.*, 2015, **2**, 041002.
18 S. Masubuchi, M. Morimoto, S. Morikawa, M. Onodera, Y. Asakawa, K. Watanabe, T. Taniguchi and T. Machida, *Nat. Commun.*, 2018, **9**, 4–6.
19 S. Masubuchi, M. Sakano, Y. Tanaka, Y. Wakafuji, T. Yamamoto, S. Okazaki, K. Watanabe, T. Taniguchi, J. Li, H. Ejima, T. Sasagawa, K. Ishizaka and T. Machida, *Sci. Rep.*, 2022, **12**, 1–7.
20 M. Onodera, Y. Wakafuji, T. Hashimoto, S. Masubuchi, R. Moriya, Y. Zhang, K. Watanabe, T. Taniguchi and T. Machida, *Sci. Rep.*, 2022, **12**, 21963.
21 Y. Wakafuji, R. Moriya, S. Masubuchi, K. Watanabe, T. Taniguchi and T. MacHida, *Nano Lett.*, 2020, **20**, 2486–2492.
22 Y. Wakafuji, M. Onodera, S. Masubuchi, R. Moriya, Y. Zhang, K. Watanabe, T. Taniguchi and T. Machida, *npj 2D Mater. Appl.*, 2022, **6**, 44.
23 D. G. Purdie, N. M. Pugno, T. Taniguchi, K. Watanabe, A. C. Ferrari and A. Lombardo, *Nat. Commun.*, 2018, **9**, 1–12.
24 L. Wang, I. Meric, P. Y. Huang, Q. Gao, Y. Gao, H. Tran, T. Taniguchi, K. Watanabe, L. M. Campos, D. A. Muller, J. Guo, P. Kim, J. Hone, K. L. Shepard and C. R. Dean, *Science*, 2013, **342**, 614–617.
25 M. Onodera, M. Arai, S. Masubuchi, K. Kinoshita, R. Moriya, K. Watanabe, T. Taniguchi and T. MacHida, *Nano Lett.*, 2019, **19**, 8097–8102.
26 A. Castellanos-Gomez, M. Buscema, R. Molenaar, V. Singh, L. Janssen, H. S. J. Van Der Zant and G. A. Steele, *2D Mater.*, 2014, **1**, 011002.
27 X. Ma, Q. Liu, D. Xu, Y. Zhu, S. Kim, Y. Cui, L. Zhong and M. Liu, *Nano Lett.*, 2017, **17**, 6961–6967.
28 G. Tai, T. Zeng, J. Yu, J. Zhou, Y. You, X. Wang, H. Wu, X. Sun, T. Hu and W. Guo, *Nanoscale*, 2016, **8**, 2234–2241.
29 B. Jiang, S. Wang, J. Sun and Z. Liu, *Small*, 2021, **17**, 1–21.
30 Z. Wu, G. Tai, R. Liu, C. Hou, W. Shao, X. Liang and Z. Wu, *ACS Appl. Mater. Interfaces*, 2021, **13**, 31808–31815.
31 A. J. Watson, W. Lu, M. H. D. Guimarães and M. Stöhr, *2D Mater.*, 2021, **8**, 032001.
32 Y.-C. Lin, W. Zhang, J.-K. Huang, K.-K. Liu, Y.-H. Lee, C.-T. Liang, C.-W. Chu and L.-J. Li, *Nanoscale*, 2012, **4**, 6637.
33 M. Amani, M. L. Chin, A. L. Mazzoni, R. A. Burke, S. Najmaei, P. M. Ajayan, J. Lou and M. Dubey, *Appl. Phys. Lett.*, 2014, **104**, 203506.
34 L. Zhang, C. Wang, X.-L. Liu, T. Xu, M. Long, E. Liu, C. Pan, G. Su, J. Zeng, Y. Fu, Y. Wang, Z. Yan, A. Gao, K. Xu, P.-H. Tan, L. Sun, Z. Wang, X. Cui and F. Miao, *Nanoscale*, 2017, **9**, 19124–19130.
35 M. A. Kang, S. J. Kim, W. Song, S. jin Chang, C. Y. Park, S. Myung, J. Lim, S. S. Lee and K. S. An, *Carbon*, 2017, **116**, 167–173.
36 Y. Cao, X. Wang, X. Lin, W. Yang, C. Lv, Y. Lu, Y. Zhang and W. Zhao, *IEEE Access*, 2020, **8**, 70488–70495.
37 P. Yang, X. Zou, Z. Zhang, M. Hong, J. Shi, S. Chen, J. Shu, L. Zhao, S. Jiang, X. Zhou, Y. Huan, C. Xie, P. Gao, Q. Chen, Q. Zhang, Z. Liu and Y. Zhang, *Nat. Commun.*, 2018, **9**, 1–10.
38 Z. Lu, L. Sun, G. Xu, J. Zheng, Q. Zhang, J. Wang and L. Jiao, *ACS Nano*, 2016, **10**, 5237–5242.
39 N. Hong, D. Kireev, Q. Zhao, D. Chen, D. Akinwande and W. Li, *Adv. Mater.*, 2022, **34**, 1–9.
40 H. Jia, R. Yang, A. E. Nguyen, S. N. Alvillar, T. Empante, L. Bartels and P. X. L. Feng, *Nanoscale*, 2016, **8**, 10677–10685.

41 K. Kang, K. H. Lee, Y. Han, H. Gao, S. Xie, D. A. Muller and J. Park, *Nature*, 2017, **550**, 229–233.
42 S. Zheng, L. Sun, X. Zhou, F. Liu, Z. Liu, Z. Shen and H. J. Fan, *Adv. Opt. Mater.*, 2015, **3**, 1600–1605.
43 W. Yan, L. Meng, Z. Meng, Y. Weng, L. Kang and X. A. Li, *J. Phys. Chem. C*, 2019, **123**, 30684–30688.
44 E. Bormashenko, I. Legchenkova, S. Navon-Venezia, M. Frenkel and Y. Bormashenko, *Appl. Sci.*, 2020, **11**, 300.
45 P. L. Sant'Ana, J. R. Ribeiro Bortoleto, N. C. da Cruz, E. C. Rangel, S. F. Durrant and W. H. Schreiner, *Polimeros*, 2020, **30**, e2020044.
46 R. Janík, M. Kohutiar, A. Dubec, M. Eckert, K. Moricová, M. Pajtášová, D. Ondrušová and M. Krbata, *Materials*, 2022, **15**, 4658.
47 C. B. Crawford and B. Quinn, *Microplastic Pollutants*, Elsevier, 2017, pp. 57–100.

